International Journal of Mechanical, Industrial and Aerospace Sciences
ISSN: 2517-9950
Vol:1, No:12, 2007

Limit Cycle Behaviour of a Neural Controller with Delayed Bang-Bang Feedback

Travis Wiens, Greg Schoenau, Rich Burton

Abstract**—** It is well known that a linear dynamic system including a delay will exhibit limit cycle oscillations when a bang-bang sensor is used in the feedback loop of a PID controller. A similar behaviour occurs when a delayed feedback signal is used to train a neural network. This paper develops a method of predicting this behaviour by linearizing the system, which can be shown to behave in a manner similar to an integral controller. Using this procedure, it is possible to predict the characteristics of the neural network driven limit cycle to varying degrees of accuracy, depending on the information known about the system. An application is also presented: the intelligent control of a spark ignition engine.

Keywords**—** Control and automation, artificial neural networks, limit cycle

I. Introduction

A commonly encountered form of limit cycle is that which results when a PID compensator is used in a system with a delay and bang-bang[1] sensor. This paper first develops equations describing this classic case, particularly for the application of fuel-air control. Next an analogous analysis is performed for the neural controller presented in [1]. A number of simplifying assumptions allow it to be shown that, for small deviations around an operating point, the training scheme operates as a integral compensator.

II. Integral Controller

The combination of a plant modelled as a gain, with a sensor including a bang-bang element and a delay is commonly given as an example of a system exhibiting a limit cycle. The analysis contained in this section is closely based on that found in [2], although similar analyses may be found in control theory textbooks. Consider the fuel-air control of a spark ignition engine via an integral controller, shown in Fig. 1. The plant is modelled as a nonlinear gain representing the fuel-air mixing function, and a delay representing the time taken for the mixture to travel from the injection point to the bang-bang oxygen sensor. The plant transfer function is thus

$$y(k) = \mathrm{F}(t_{inj}(k-d)) \tag{1}$$

where y is the oxygen sensor output, $\mathrm{F}(.)$ is a nonlinear bang-bang function, t_{inj} is the fuel injector pulse width, k is the index of the sample, and d is the delay (in units of injection events).

Authors are with the Department of Mechanical Engineering, University of Saskatchewan, Saskatoon, Canada.

[1]A bang-bang sensor is a two-value sensor. For example, the oxygen sensor in a vehicle produces one voltage when the fuel-air ratio is lean and another when it is rich, but little information in between

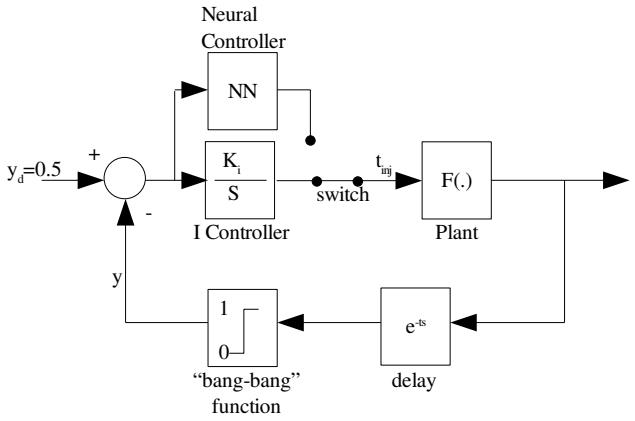

Fig. 1. Block diagram of the system described in this paper (in the Laplace domain). The switch allows the control to to chosen from either an integral controller or a neural network controller.

A discrete time integral controller is used to control the fuel-air ratio such that it oscillates about the stoichiometric ratio[2] which corresponds to the sensor's transition point. The controller is given by the function

$$t_{inj}(k) = \begin{cases} t_{inj}(k-1) + K_{ir} & y(k) > y_t \\ t_{inj}(k-1) + K_{il} & y(k) < y_t \end{cases} \tag{2}$$

where K_{ir} is the rich integral gain (negative), K_{il} is the lean gain, and y_t is the transition point of the sensor.

The resulting waveform will be a triangular wave with the upward slope equal to K_{il} and the downward slope equal to K_{ir}, as shown in Fig. 2. Because of the delay, the pulse width will overshoot the stoichiometric pulse width for d samples. Thus the rich peak of the curve will be approximately $K_{il}d$ above the stoichiometric pulse width, t_{is}, and the trough will be $-K_{ir}d$ below. This is an approximate value, as depending on the conditions, each section may be $d+1$ samples long rather than d. This is true throughout the analyses in this paper. If matching integral gains are used (i.e. $K_{il} = -K_{ir}$) the time taken for the pulse width to recover from the peak back to stoichiometry will be the same as the time taken to reach the peak, d. Thus, the period of the limit cycle will be $4d$ [2]. If unsymmetrical gains are used, the period, P, can be shown to be

$$P = d\left(2 + \left|\frac{K_{il}}{K_{ir}}\right| + \left|\frac{K_{ir}}{K_{il}}\right|\right). \tag{3}$$

[2]The stoichiometric ratio is the ratio of fuel to air such that there is just enough oxygen to completely combust the fuel.

as shown in Fig. 3. These unsymmetrical integral gains can be used to bias the fuel-air ratio rich or lean. By integrating the triangles, it can be shown that the mean deviation from stoichiometry is given by

$$\overline{t_{inj} - t_s} = \frac{d}{2}(K_{il} + K_{ir}) \tag{4}$$

and the peak to peak magnitude of the oscillations will be

$$\max(t_{inj}) - \min(t_{inj}) = d(K_{il} - K_{ir}). \tag{5}$$

Plots of (3) and (4) are presented in Fig. 4 and 5. For ease of comparison, the root mean squared error of this curve from the stoichiometric point is

$$RMSE = \left(\frac{d^2}{3\left(2 - \frac{K_{il}}{K_{ir}} - \frac{K_{ir}}{K_{il}}\right)} \left[K_{il}^2 \left(1 - \frac{K_{il}}{K_{ir}}\right) + \ldots \right. \right. \\ \left. \left. K_{ir}^2 \left(1 - \frac{K_{ir}}{K_{il}}\right) \right] \right)^{\frac{1}{2}}. \tag{6}$$

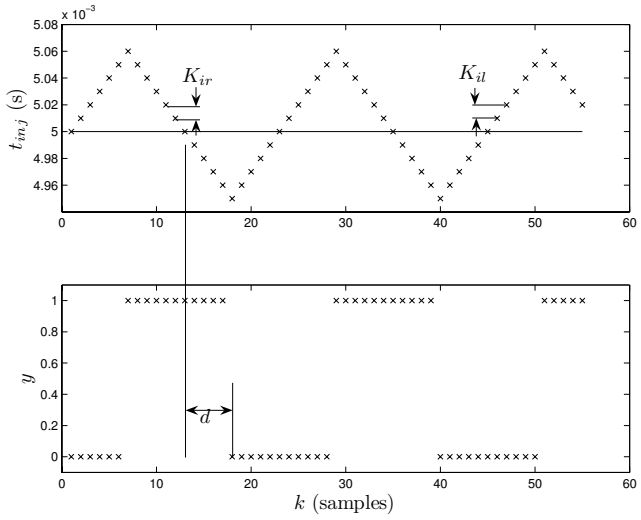

Fig. 2. Limit cycle behaviour in a system with symmetric parameters $K_{ir} = -0.01$ ms and $K_{il} = 0.01$ ms. Notice that the period of the waveform is approximately $4d$. The stroichiometric pulse width is 5.0 ms and the delay is 5 samples.

Therefore, if one knows the delay of the system and the desired bias and period of oscillations for proper catalyst operation, one can solve for K_{il} and K_{ir} by using (3) and (4) to yield

$$K_{ir} = \frac{\overline{t_{inj} - t_s}}{d} \left(\frac{\frac{P}{d} - 4 \pm \sqrt{-4\frac{P}{d} + \left(\frac{P}{d}\right)^2}}{\frac{P}{d} - 4} \right) \tag{7}$$

$$K_{il} = 2\frac{\overline{t_{inj} - t_s}}{d} - K_{ir} \tag{8}$$

III. Neural Controller

A similar analysis can be performed on the neural controller presented in [1]. This controller uses a type of inverse model

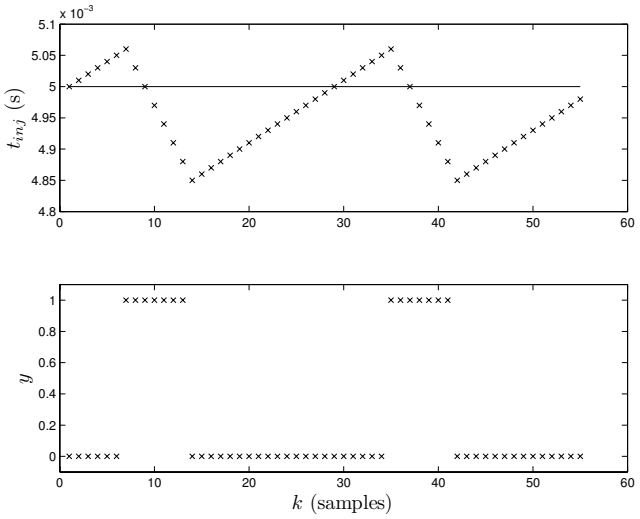

Fig. 3. Limit cycle behaviour in a system with unsymmetrical integral gains $K_{ir} = -0.03$ ms, $K_{il} = 0.01$ ms. Although the delay is the same, the period has increased. The unsymmetrical gains allow the fuel air ratio to biased, lean in this case.

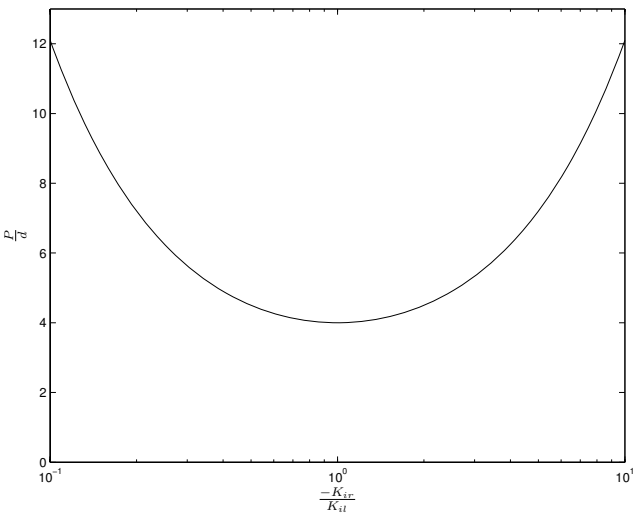

Fig. 4. The period of oscillations for an integral controlled system has a minimum when $K_{ir} = -K_{il}$ and increases as the ratio of integral gains changes. This is a plot of (3).

control to determine an estimate of the stoichiometric injection pulse width. It does this by first identifying the engine using a two-part model.

The first part is a a non-linear, but static classifier, which estimates whether the mixture in the intake (no delay) would be rich or lean, given inputs of intake manifold pressure, P_m, engine speed, N_e, and injector pulse width t_{inj}. This part of the model takes the form of a generalized neural network[3] which is updated via online backpropagation training[4] with feedback from the oxygen sensor in the exhaust. This type of network uses the same neurons as a multilayer perceptron, but instead of being organized in layers, it is organized in a row, as shown in Fig. 6. Each neuron has inputs coming from the

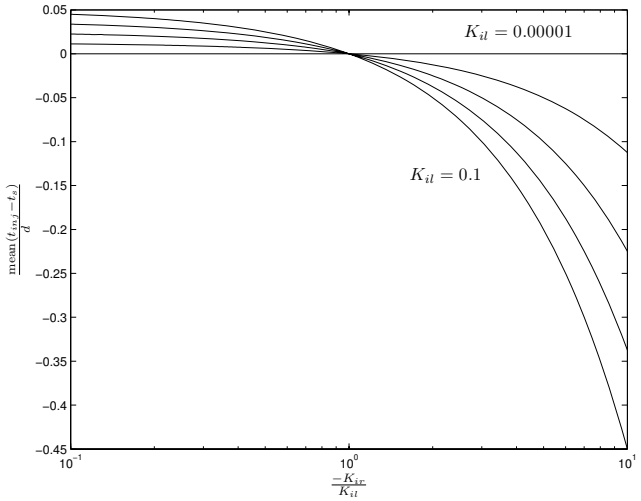

Fig. 5. According to (4), the mean injector pulse width may be biased, as shown in this figure. In all cases, the bias is zero when $K_{ir} = -K_{il}$.

outputs of the neurons to its left.

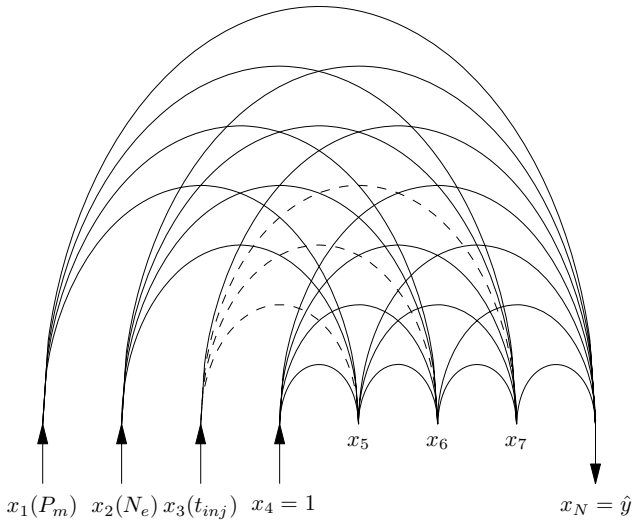

Fig. 6. The generalized neural network architecture uses a string of neurons instead of layers. Each neuron has inputs coming from the neurons to its left. The weights connecting t_{inj} to the hidden neurons (shown with dashed lines) are set to zero to allow the network to be inverted.

The second part of the network is a pure time delay. Since the delay changes based on a number of factors, the model's estimate of the delay is taken to be a range between a minimum and maximum value. The delay model is used to match the delayed oxygen sensor reading to the appropriate inputs. The training algorithm skips any point at which the proper oxygen sensor reading is uncertain. After the training phase is complete, the controller is required to solve the model equations for the stoichiometric pulse width, given the current values for P_m and N_e. By strategically zeroing weights, this can be done algebraically. Further details of the control scheme may be found in [1] and [5].

The learning equation for any arbitrary weight W_i, in the neural network is

$$W_i(k) = W_i(k-1) - \eta \frac{\mathrm{d}E}{\mathrm{d}W_i} \tag{9}$$

where η is the learning rate and the error term, E, is

$$E = \frac{1}{2}(\hat{y} - y)^2 \tag{10}$$

where $\hat{y}$ is the network's estimate of the bang-bang sensor's output y.

The error gradient can be found by starting at the equation for the the output neuron:

$$\hat{y} = x_N = \mathrm{sig}(\sigma) \tag{11}$$

$$\sigma = W_1 x_1 + W_2 x_2 + ...W_{N-1} x_{N-1} \tag{12}$$

where $\mathrm{sig}(.)$ is a unipolar sigmoidal function and x_i is the output of the ith neuron of a total of N neurons.

The gradient can be rewritten as

$$\frac{\mathrm{d}E}{\mathrm{d}W_i} = \frac{\mathrm{d}E}{\mathrm{d}\hat{y}} \frac{\mathrm{d}\hat{y}}{\mathrm{d}\sigma} \frac{\mathrm{d}\sigma}{\mathrm{d}W_i} \tag{13}$$

using the chain rule, and (10), (11) and (12) may be differentiated as

$$\frac{\mathrm{d}E}{\mathrm{d}\hat{y}} = \hat{y} - y \tag{14}$$

$$\frac{\mathrm{d}\hat{y}}{\mathrm{d}\sigma} = \mathrm{sig}(\sigma)(1 - \mathrm{sig}(\sigma)) \tag{15}$$

$$= \hat{y}(1 - \hat{y}) \tag{16}$$

$$\frac{\mathrm{d}\sigma}{\mathrm{d}W_i} = x_i, \tag{17}$$

so

$$\frac{\mathrm{d}E}{\mathrm{d}W_i} = (\hat{y} - y)\hat{y}(1 - \hat{y})x_i. \tag{18}$$

An important thing to notice is that the neural network is inverted to find its estimate of the stoichiometric pulse width, so $\hat{y} \approx 0.5$ for any operating point it controls. Also, since the sensor is a bang-bang sensor, it only has two possible values (0 or 1). Therefore, (18) may be simplified as

$$\frac{\mathrm{d}E}{\mathrm{d}W_i} = (\pm 0.5)(0.5)(1 - 0.5)x_i \tag{19}$$

$$\frac{\mathrm{d}E}{\mathrm{d}W_i} = \pm \frac{1}{8} x_i. \tag{20}$$

Now consider the effect of this change on the next injection t_{inj}. By inverting the network (see [1]), the scaled pulse width is given by

$$x_3 = \frac{-1}{W_3}(W_1 x_1 + W_2 x_2 + W_4 x_4 + W_5 x_5 + \ldots W_{N-1} x_{N-1}) \tag{21}$$

where

$$t_{inj} = x_3 t_{isc} + t_{ios} \tag{22}$$

with t_{isc} and t_{ios} as constant scaling factors for t_{inj} such that the range of x_3 is constrained to the range of 0 to 1, and x_1 and x_2 are network inputs: manifold pressure and engine speed, also scaled to the range of 0 to 1. x_4 is set to 1 to provide a bias.

If ϵ is defined as the difference $\hat{y} - y$, which would correspond to the control error in a PID controller, the linearized transfer function for the training algorithm can be expressed by $\frac{\mathrm{d}t_{inj}}{\mathrm{d}\epsilon}$, which is

$$\frac{\mathrm{d}t_{inj}}{\mathrm{d}\epsilon} = \sum_{i=1}^{N-1} \frac{\mathrm{d}t_{inj}}{\mathrm{d}x_3} \frac{\mathrm{d}x_3}{\mathrm{d}W_i} \frac{\mathrm{d}W_i}{\mathrm{d}\epsilon} \tag{23}$$

if one assumes that the effect of the hidden weights is negligible (because of their indirect influence on the output). This linearized analysis is only valid for small deviations about an operating point. The terms in this equation can be found by differentiation. Substituting (19) into (9), the result is

$$W_i(k) = W_i(k-1) - \eta\epsilon\frac{1}{4}x_i \tag{24}$$

which is differentiated as

$$\frac{\mathrm{d}W_i}{\mathrm{d}\epsilon} = -\eta\frac{1}{4}x_i. \tag{25}$$

The differentiation of (21) can be shown to be

$$\frac{\mathrm{d}x_3}{\mathrm{d}W_i} = \frac{-x_i}{W_3}. \tag{26}$$

Finally, (22) can be differentiated as

$$\frac{\mathrm{d}t_{inj}}{\mathrm{d}x_3} = t_{isc} \tag{27}$$

By substituting (25), (26) and (27) into (23), the result is

$$\frac{\mathrm{d}t_{inj}}{\mathrm{d}\epsilon} = \frac{\eta t_{isc}}{4W_3} \sum_{i=1}^{N-1} x_i^2. \tag{28}$$

Again, since the value of $\hat{y}$ is constrained to 0.5 and y is contrained to 0 or 1, ϵ must equal ± 0.5. Thus if one assumes that the system is linear for small deviations about $\epsilon = 0$, $\mathrm{d}\epsilon = \pm 0.5$ and the rate of change of the pulse width from one injection to the next is

$$\mathrm{d}t_{inj} = \pm\frac{\eta t_{isc}}{8W_3} \sum_{i=1}^{N-1} x_i^2. \tag{29}$$

This provides good results compared to simulation data where all the neuron outputs x_i were known.

If one wishes to predict the performance of a controller, it is necessary to estimate the values for the hidden neurons. If one assumes that the values for $x_5, x_6..x_{N-1}$ are uniformly distributed between 0 and 1, the sum can be estimated[6] to be

$$\sum_{i=5}^{N-1} x_i^2 \approx \frac{N-5}{3}. \tag{30}$$

Thus, if one knows the scaled values for the intake manifold pressure (x_1), engine speed (x_2) and injector pulse width (x_3), and remembering that $x_4 = 1$, then (29) can be written as

$$\mathrm{d}t_{inj} = \pm\frac{\eta t_{isc}}{8W_3}\left(x_1 + x_2 + x_3 + 1 + \frac{N-5}{3}\right). \tag{31}$$

One further simplification can be made if one does not know the operating point a priori. In this case, the values for x_1, x_2, and x_3 are also assumed to be uniformly distributed over the range of 0 to 1 and the result is

$$\mathrm{d}t_{inj} = \pm\frac{\eta t_{isc}}{8W_3}\left(1 + \frac{N-1}{3}\right). \tag{32}$$

Any of (29), (31), or (32) give reasonable results; of course, greater accuracy may be obtained as more information is utilized.

Note that $\mathrm{d}t_{inj}$ in the above equations plays the same role as K_{il} and K_{ir} in a proportional controller and their values can be directly compared. However the waveform is slightly different. As mentioned above, the training scheme tries to match the neural inputs to the proper delayed feedback value. However, since there is uncertainty in the estimate of the delay, there are times when the training scheme must skip a number of points. Therefore, instead of being a triangular waveform, the waveform has "plateaus", level spots at each peak and valley in t_{inj}. Due to these points being ignored by the training scheme, the limit cycle frequency is decreased and the mean deviation from stoichiometry is increased. If the slope of each of these sections is $\mathrm{d}t_{inj}$, and the range of possible delays values is r, then the root mean squared error from the stoichiometric pulse width will be

$$RMSE = d\mathrm{d}t_{inj}\sqrt{\frac{\frac{4}{3}d + 2r}{4d + 2r}} \tag{33}$$

and the period is

$$P = 4d + 2r. \tag{34}$$

Note that, as with the integral controller, these values are approximate as the length of time taken for each section can be $d + 1$ samples, rather than d.

It is also possible to bias the control scheme by using different learning rates for lean and rich operation, in the same way as different integral gains may be used to bias the fuel-air ratio.

IV. Experimental Verification

The controller described above was implemented on a 2001 GM 2500HD truck, fuelled by natural gas (further details may be found in [7]). This truck has a Vortec 6L V8 engine, with each bank controlled independently. The original engine control unit (ECU) maintained control of all functions except fuel control (i.e. spark timing, idle air control, etc.). The controller was programmed such that the relevant parameters could be easily adjusted to examine their effects. For each trial, the truck was run at idle for 60 seconds and data was recorded from the eight injectors, as well as the two heated oxygen sensors, the intake manifold pressure transducer, and a wide-range oxygen sensor. This data was recorded at a rate of 200 kSamples/s. Note that the "bang-bang" heated oxygen sensors were used for feedback and training; the wide-range oxygen sensor's measurements were only used for evaluation of the controller and were not used in its algorithm. All tests were performed with the engine, oxygen sensors and catalysts at their operating temperature.

The first test performed was to determine the effect of the integral gain. The controller was set up with $K_{ir} = -K_{il} =$

K_i and $\eta = 0$ to eliminate the effects of the neural network. Fig. 7 shows the aggregated results of the amplitude of the limit cycle over a variety of integral gains, along with the theoretical curve from (6). One can see that the shape of the curve is accurate for K_i values greater than 0.01 ms, although there is an approximately constant bias error of 0.09 ms. This bias may be due to fluctuations in the operating point which may be attributed to spark timing or idle air control oscillations. Below $K_i = 0.01$ ms these other fluctuations dominate and the integral controller does not cause the same limit cycle.

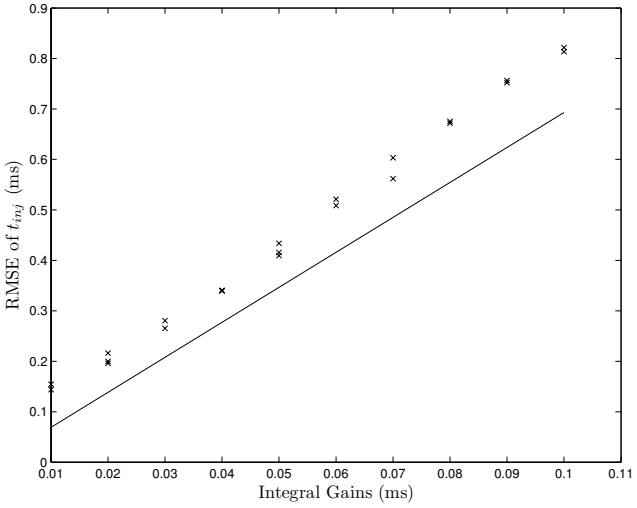

Fig. 7. Effect of integral gain on oscillation amplitude, measured by the standard deviation of 60 seconds of idling at each data point. The integral gains are symmetric ($K_{il} = -K_{ir} = K_i$). These values may be compared to the theoretical value from (6), shown as the solid line.

Fig. 8 demonstrates the ability to bias the controller via asymmetric integral gains. The rich integral gain was held constant at -0.01 ms and the lean integral gain was varied. This test was again performed at idle (the mean t_{inj} was approximately 4.85 ms) with the neural learning algorithm disabled. Fig. 9 shows the period of the limit cycle oscillations, compared to the theoretical curve from (3). Finally Fig. 10 shows an example of the resultant relative fuel-air ratio, λ, defined as

$$\lambda = \frac{m_{is}}{m_i}, \tag{35}$$

where m_i is the mass of fuel injected and m_{is} is the stroichiometric pulse width. Notice the different slopes of the increasing and decreasing portions of the trace.

The next test was performed to verify the theoretical equations for the neural system. In this test the integral controller was disabled and the learning rate, η, was varied. Fig. 11 shows the effect of learning rate on the oscillation magnitude (as quantified by the root mean squared error in pulse width), compared to the results of (33). Fig. 12 shows a sample waveform. Again, the results follow the shape of the theoretical curve for η greater than 0.005, with similar errors as in Fig. 7.

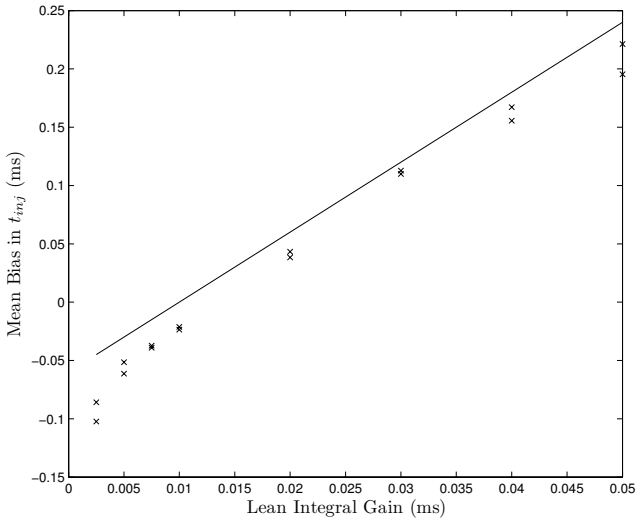

Fig. 8. Effect of asymmetric integral gain on the mean pulse width. The rich integral gain, K_{ir}, is held constant at -0.01 ms while the lean gain, K_{il}, is varied.

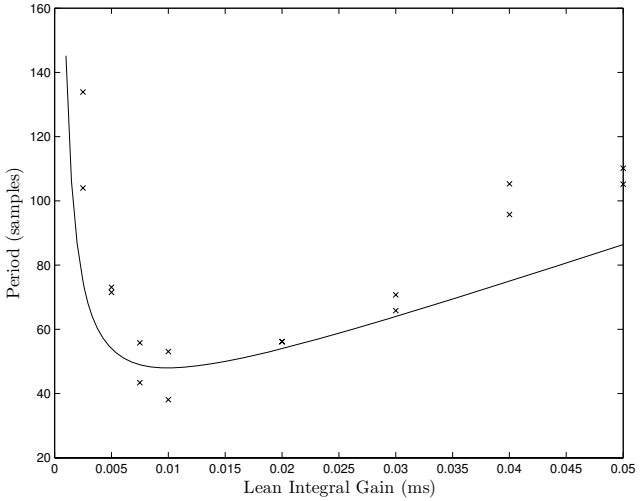

Fig. 9. Effect of asymmetric integral gain on the period of the limit cycle oscillations. The rich integral gain, K_{ir}, is held constant at -0.01 ms while the lean gain, K_{il}, is varied.

V. Conclusion

This paper developed equations showing that the training dynamics of the neural controller can be expressed in a linearized form. In particular, it is possible to determine the period, amplitude and bias of the limit cycle of a particular training scheme using "bang-bang" feedback for online training. This development demonstrates that the dynamics of the training scheme parallel those of a classical linear integral controller, and much of the same analysis may be performed. Although there were some errors between the theoretical and experimental values, the theory was verified via experiments performed on a system used to control the fuel-air ratio of a spark-ignition engine.

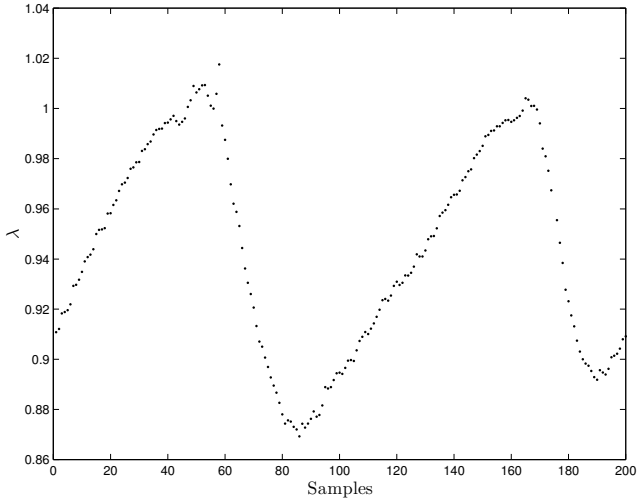

Fig. 10. A sample of the relative air-fuel ratio waveform produced with $K_{ir} = -0.01$ ms and $K_{il} = 0.05$ ms. Note the differing slopes of the increasing and decreasing portions of the trace.

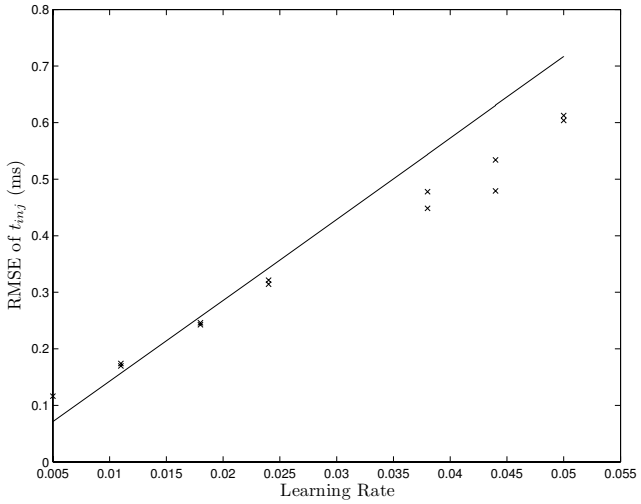

Fig. 11. Effect of learning rate, η, on the amplitude of oscillations.

VI. Acknowledgement

The authors would like to acknowledge the financial support of NSERC; the Saskatchewan Research Council for providing equipment and expertise; and General Motors Alternative Fuels for the loan of the test vehicle. Thanks are also given to Natural Resources Canada and Precarn Inc who funded initial work in this area.

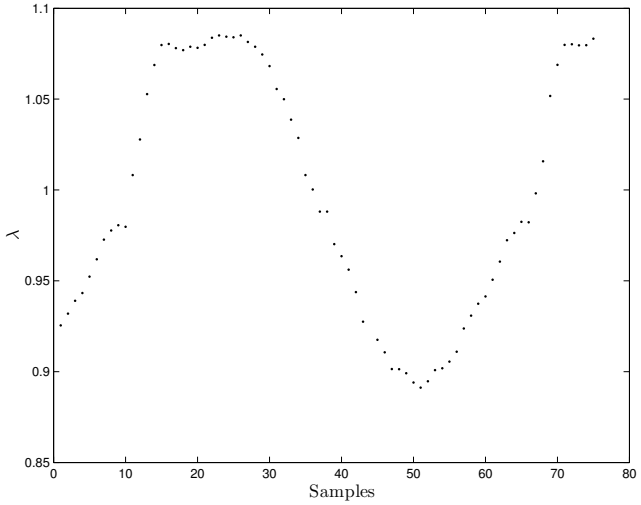

Fig. 12. A sample of the relative air-fuel ratio waveform produced with $\eta = 0.05$.

References

[1] T. Wiens, R. Burton, G. Schoenau, and M. Sulatisky, "Intelligent fuel air ratio control of gaseous fuel SI engines," Tech. Rep. MISC-0168, Saskatchewan Research Council, Saskatoon, 2006.
[2] J. Heywood, *Internal Combustion Engine Fundamentals*. New York: McGraw Hill, 1988.
[3] P. Werbos, "Backpropagation Through Time: What It Does and How to Do it," in *Proceedings of the IEEE*, vol. 78, pp. 1550–1560, 1990.
[4] D. Saad, ed., *On-line Learning in Neural Networks*. Cambridge: Cambridge University Press, 1998.
[5] T. Wiens, R. Burton, and G. Schoenau, "Algebraic inversion of an artifcial neural network classifer," in *Proceedings of the European Symposium on Artificial Neural Networks*, (Bruges), 2007.
[6] D. Zwillinger, *CRC Standard Mathematical Tables and Formulae*. Boca Raton: Chapman & Hall/CRC press, 2002.
[7] T. Wiens, R. Burton, G. Schoenau, M. Sulatisky, S. Hill, and B. Lung, "Preliminary experimental verification of an intelligent fuel air ratio controller," Tech. Rep. 2007-01-1339, Society of Automotive Engineers (SAE), 2007.